Journal of Computational Applied Mechanics 2024, 55 (2): 144-164

DOI: 10.22059/JCAMECH.2023.366355.886

RESEARCH PAPER

Analyzing the Thermoelastic Responses of Biological Tissue Exposed to Thermal Shock Utilizing a Three-Phase Lag Theory

Ashraf M. Zenkour [a,b,*], Tariq Saeed [b,c], Amal M. Aati [a,d]

[a] *Department of Mathematics, Faculty of Science, King Abdulaziz University, Jeddah 21589, Saudi Arabia*
[b] *Department of Mathematics, Faculty of Science, Kafrelsheikh University, Kafrelsheikh 33516, Egypt*
[c] *Financial Mathematics and Actuarial Science (FMAS)-Research Group, Department of Mathematics, Faculty of Science, King Abdulaziz University, Jeddah 21589, Saudi Arabia*
[d] *Department of Mathematics, College of Arts and Science in Rijal Alma and the Applied branch, King Khalid University, Abha 61421, Saudi Arabia*

Abstract

This article presents a mathematical analysis of thermoelastic skin tissue using an improved thermal conduction theory known as the refined three-phase-lag (TPL) theory. By accounting for the effects of multiple time derivatives, this advanced model provides a more accurate representation of how skin tissue behaves under different temperature conditions. The thin skin tissue is considered to have mechanically clamped surfaces, which are assumed to be one-dimensional. Furthermore, the skin tissue experiences a thermal shock load on its outer surface while maintaining a constant temperature on its inner surface. The proposed model has led to the derivation of certain generalized thermoelasticity theories in previous studies. The Laplace transform and its associated numerical inversion method are employed to calculate the distributions of temperature, displacement, dilatation, and stress in the system. The obtained outcomes are explicitly depicted to analyze the significant influences on the distributions of the field variables. These findings shed light on the behavior of skin tissue when subjected to a particular temperature distribution at the boundary condition, enhancing our knowledge in this area.

Keywords: Refined TPL theory; bio-thermal; skin tissue; thermal shock.

1. Introduction

The temperature gradient is presumptively proportional to the heat flux in the traditional theory of heat conduction, which Fourier first proposed. The conventional Fourier heat conduction equation implies an infinite speed of heat propagation, which does not align with the observed phenomena in experiments [1]. Although Fourier's law is suitable for describing heat conduction in a steady state, it fails to capture the transient thermal response, high-temperature gradients, and intense heat flux. To accurately account for these phenomena, the non-Fourier effect must be incorporated. To overcome the issue of infinite heat propagation speed, an alternative approach was introduced through the development of the single-phase-lag (SPL) theory or Cattaneo–Vernott (C–V) theory [2, 3], which utilizes a hyperbolic heat equation as an alternative approach. Furthermore, Tzou [4] proposed the dual-phase-lag theory (DPL), which incorporates two relaxation times to effectively capture the phase-lagging behavior exhibited by both temperature gradient and heat flux. Later, scientists came up with the three-phase-lag model (TPL) to explain more complicated behavior by adding another phase lag to the thermal displacement gradient [5]. All of these non-Fourier

* Corresponding author.
E-mail address: zenkout@kau.edu.sa

models rely on the expansion of Taylor's series with integer-order derivatives. To enhance the accuracy and realism of these models, further comprehensive research is required to experimentally measure the relaxation time for different materials.

Furthermore, it is important to consider not only heat conduction but also the effects of heat-induced displacement and stress [6]. These factors have a significant impact on the response of biological tissues during treatment. By taking into account these additional factors, we can gain a more comprehensive understanding of thermal behavior and improve therapeutic outcomes. Biot advanced the classical thermoelastic theory by incorporating the impact of displacement on temperature using Duhamel–Neumann equations. This resulted in the establishment of a coupling relationship between temperature and elastic displacement, enhancing our understanding of thermal-mechanical interactions [7]. Biot's theory still relies on Fourier heat conduction, which assumes an infinite heat propagation velocity. To address this limitation, various generalized thermoelastic theories have been proposed and extensively investigated as potential solutions to overcome this drawback. Lord and Shulman were the pioneers in proposing the first generalized thermoelastic theory, known as the L–S model. This model is based on the SPL heat conduction approach [8]. Green and Lindsay (G–L) expanded upon Biot's theory by incorporating two-phase lags and introducing the concept of temperature rate [9]. Hetnarski and Ignaczak (H–I) proposed a non-linear relationship between temperature and elastic response, demonstrating their interdependence [10]. Green and Naghdi examined two distinct thermoelastic theories that incorporate the finite heat propagation velocity, namely the Green–Naghdi (G–N) theory type II and type III [11, 12].

In medical thermal therapeutic applications, it is important to accurately model and understand how heat is transported within biological tissues and organs and its consequences. By developing mathematical models and computational simulations based on principles of thermodynamics and fluid dynamics, researchers can gain insights into how heat spreads throughout the body during thermal therapies. Despite the significance of studying the mechanical effects on biological tissues, there is a prevailing tendency in many studies to solely focus on analyzing the thermal effects. This limited approach overlooks a comprehensive understanding of how mechanical factors contribute to tissue behavior. Marin et al. [13] investigated the nonlinear hyperbolic bioheat equation under different boundary conditions to analyze its application in medicinal treatments using the finite element technique. Al-Lehaibi [14] conducted a study using the DPL model to explore the response of skin tissue to a continuous flow of surface heat generated by a constant-voltage electrical current. The study revealed that key variables such as voltage, resistance, electric shock duration, and DPL play a crucial role in determining the distribution of temperature rise within the skin tissue. Sharma and Kumar [15] utilized a complex non-linear DPLBHT model to analyze the temperature distribution in skin tissues during hyperthermia treatment of infected cells. To solve this challenging non-linear problem, the researchers applied the FERK (4,5) method for accurate calculation of results. Youssef and Alghamdi [16] employed the TTDPL model to examine the response of skin tissue when subjected to a constant heat flux on its surface. Their investigation revealed that variations in the time parameter, heat flux value, and two-temperature parameter all exert significant influences on temperature changes within the tissue.

Zhang et al. [17] examined the thermal response of skin tissue using a TPL model. An analytical solution was obtained by adopting the method of separation of variables, revealing that the temperature behavior predicted by the TPL model falls between that of the C–V model and the DPL model. Hobiny et al. [18] put forward an analytical approach utilizing Laplace transforms and experimental validation to assess thermal damage and temperature resulting from laser irradiation on the skin surface. Their study also demonstrates the effectiveness of the TPL bioheat mathematical model as a valuable tool for estimating bioheat transfer in skin tissue. Verma and Kumar [19] aimed to predict how temperature is distributed in biological tissue by using a TPL bioheat model. Employed the Gaussian radial basis function (RBF) and Crank–Nicolson (C–N) scheme as approximation methods for spatial and time derivatives, respectively. Also, the study analyzed the influence of phase lag and heating frequency on temperature distribution in tissue under different surface heating conditions. Kumara and Raia [20] employed the semi-analytical approach to solve the TPL bioheat transfer model, which was subsequently verified using experimental data. Verma and Kumar [21] utilized the TPL bioheat model to investigate the phase change occurring in skin tissue during cryosurgery and also developed an effective numerical algorithm based on heat capacity for solving the governing equation. The estimation of space derivatives was achieved using RBF, while time derivatives were computed using the finite difference method (FDM). Sur et al. [22] conducted a study on modeling the bioheat equation by incorporating the memory-dependent derivative (MDD) and a TPL model within the framework of the two-temperature theory. Researchers also specifically examined how the MDD and velocity of a moving heat source impact skin tissue temperature using Laplace transform techniques. Kumari and Singh [23] formulated a mathematical model to investigate the thermal behavior within living tissue, employing the space-fractional approach and a TPL constitutive relation. Singh et al. [24] introduced a three-dimensional non-Fourier bio-heat transfer model specifically designed for cardiac ablation procedures based on a TPL approach and employed COMSOL multiphysics software to forecast temperature distributions and ablation volumes. The researchers further assessed the accuracy and reliability

of their model by comparing it with analytical findings from previous studies in the literature.

Several researchers have explored the coupled heat transfer phenomena in biological tissues using Fourier, SPL, and DPL models. These investigations have considered the thermal and mechanical effects of tissue and incorporated various modeling assumptions. To the authors' knowledge, there are only a few articles in the literature that discuss the TPL bioheat model. Li et al. [25] investigated the thermo-mechanical behaviors of triple-layered skin tissue, considering the influence of a variable blood perfusion rate by employing generalized bio-thermoelastic theories. Their study emphasizes that it is crucial to account for the variability in blood perfusion rate when analyzing burn and thermal therapy effects on skin tissue. Neglecting this variability can result in an overestimation of field quantities. Hobiny and Abbas [26] utilized the fractional SPL model to investigate how fractional time derivatives impact the interaction between heat and mechanical behavior in living tissue during hyperthermia treatment. The study also involved applying both the eigenvalues approach and analytical techniques to obtain solutions for various field quantities. Sobhy and Zenkour [27] introduced a mathematical model that accounts for the thermoelastic behavior of skin tissue by utilizing a refined Lord–Shulman (L–S) heat conduction theory. Zenkour et al. [28] proposed a novel model for thermoelasticity in thin skin tissue, drawing inspiration from the G–L generalized thermoelasticity theory. Their refined model takes into account various factors that contribute to the behavior of heat and mechanical response in the skin tissue, providing a more comprehensive understanding of its thermomechanical properties.

Li et al. [29] examined the behavior of biological tissue during cryosurgery and employed a DPL theory to investigate this phenomenon. The study aimed to gain insights into the complex dynamics associated with this process. Tiwari et al. [30] proposed a novel bio-heat transfer model for the thermal therapy of skin tissue, which incorporated memory-dependent derivatives and DPL to accommodate various thermal conditions like thermal shock and harmonic-type heating. Their study revealed that integrating the memory effect into this unified model greatly improved its capability to accurately predict field quantity data during diverse thermal treatment procedures. Hu et al. [31, 32] developed a unique bioheat conduction model based on the time-fractional DPL approach. This model was employed to analyze the thermoelastic response of skin tissue under sudden temperature shocks. Additionally, they used the same model to investigate the response of biological tissue when subjected to hyperthermia treatment using laser heating that moves across the tissue. Ezzat [33] formulated a thermo-viscoelasticity theory by integrating fractional DPL with the rheological properties of the volume. The objective was to examine the effects of this theory on one-dimensional bioheat transfer and analyze the resulting heat-induced mechanical response. Zenkour et al. [34] performed a mathematical analysis on thermoelastic skin tissue using a refined DPL theory that focused on one-dimensional skin tissue with surfaces that are mechanically clamped. Zhang et al. [35] utilized a generalized thermoelasticity model with three phase lag times and employed the Laplace transform and numerical inverse transform methods to examine the dynamic response of biological tissues to sudden temperature changes.

This article aims to investigate the thermoelastic response of biological tissue subjected to thermal shock using the refined TPL theory. The simple TPL, DPL, SPL, G–N III, and CTE theories are also shown. The objective is to provide an explanation for a 1D problem and advance a novel generalized bio-thermal model. The impacts of various factors such as the thermal shock parameter, relaxation times, blood perfusion rate, time points, and thermal conductivity (including its rate) on different field quantities within skin tissue are investigated and illustrated through figures.

2. Basic equations

The model of classical coupled thermoelasticity (CTE) was presented by Biot [7], which is based on Fourier's law and the energy conservation equation,

$$q_i(x,t) = -k_t \theta_{,i}(x,t), \tag{1}$$

$$\rho_t c_t \dot{\theta} + \gamma_t T_0 \dot{e} = -q_{i,i} + Q. \tag{2}$$

Fourier's law connects the heat flux $q_i(x,t)$ to the temperature gradient $\theta_{,i}(x,t)$ at the arbitrary point of tissue and k_t denotes the thermal conductivity of the tissue. $\theta = T - T_0$ represents the temperature increment, where T and T_0 describe the absolute temperature and reference temperature of the ambient, respectively. Besides, the comma $(,)$ in the lower right position signifies differentiation with respect to spatial coordinates, while the dot $(.)$ in the upper position represents differentiation with respect to time.

In the energy conservative equation Eq. (2), ρ_t and c_t are used to represent the mass density and specific heat capacity per unit mass of tissues, respectively. The thermal modulus γ_t is defined with the thermal expansion coefficient α_t as $\gamma_t = (2\mu_t + 3\lambda_t)\alpha_t$, in which λ_t and μ_t are Lamé's constants specific to the tissue. $e = e_{kk}$ denotes volumetric strain, e_{ij} represents the strain tensor, and Q is the term used to describe the heat input per unit volume.

In Eq. (2) of the energy conservation equation, the impact of the rate at which volumetric strain occurs on

temperature ($\gamma_t T_0 \dot{e}$) is also accounted for. If we disregard the effect of the rate of volumetric strain (e), the energy conservation equation mentioned above can be simplified to align with the classical heat conservation equation commonly utilized in Pennes' widely accepted heat transfer model [36].

While classical thermoelasticity theory is commonly employed in engineering for its simplicity and effectiveness, certain materials like sand and biological tissue exhibit non-Fourier phenomena. As a result, a coupled theory based on Fourier's conduction law has been developed to account for these thermal behaviors. To account for the occurrence of phase lag in the bioheat transfer process, Cattaneo [2] and Vernotte [3] introduced a relaxation time τ_q into the heat conduction equation as

$$q_i\left(x, t+\tau_q\right) = -k_t \theta_{,i}(x,t). \tag{3}$$

The modified model demonstrates that, at a specific location, the heat flux and temperature gradient occur at different times, where τ_q is the PL for the heat flux vector. Also, this theory is referred to as the L–S thermoelasticity theory. Afterward, Tzou [37, 38] suggested a DPL model by introducing two relaxation times. Under this theory, Fourier's law is replaced with

$$q_i\left(x, t+\tau_q\right) = -k_t \theta_{,i}(x, t+\tau_\theta), \tag{4}$$

in which the relaxation time τ_θ in this context signifies the phase lag of the temperature gradient. and $(0 \le \tau_\theta < \tau_q)$.

Without the need for a relaxation time, Green and Naghdi [11, 12] proposed another generalized thermoelasticity model that is capable of directly accommodating the non-Fourier effect of thermal propagation. Consequently, the G–N II and G–N III thermoelastic theories were introduced as alternative models. These models introduce a new variable known as thermal displacement (ϑ), which is defined by the equation $\dot{\vartheta} = \theta$ to describe its connection with temperature. In a manner akin to Fourier's law of heat conduction, the heat conduction equations for G–N II and III were established as follows

$$q_i(x,t) = -k_t^* \vartheta_{,i}(x,t), \tag{5}$$

$$q_i(x,t) = -\left[k_t \theta_{,i}(x,t) + k_t^* \vartheta_{,i}(x,t)\right], \tag{6}$$

in these models, the parameter k_t^* represents the rate of thermal conductivity. Using the G–N III thermoelasticity as a foundation, Choudhuri [5] proposed a new model that incorporates a three-phase lag. As a result, the generalized equation for heat conduction can be expressed as

$$q_i\left(x, t+\tau_q\right) = -\left[k_t \theta_{,i}(x, t+\tau_\theta) + k_t^* \vartheta_{,i}(x, t+\tau_\vartheta)\right], \tag{7}$$

where τ_ϑ represents a PL of thermal displacement gradient with $(0 \le \tau_\vartheta < \tau_\theta < \tau_q)$.

Now, if we expand the above equation by applying Taylor's series up to the higher-order terms in τ_q, τ_θ, and τ_ϑ [39-42], we yield

$$-\left[k_t\left(1+\sum_{m=1}^{M_1}\frac{\tau_\theta^m}{m!}\frac{\partial^m}{\partial t^m}\right)\theta_{,i} + k_t^*\left(1+\sum_{m=1}^{M_1}\frac{\tau_\vartheta^m}{m!}\frac{\partial^m}{\partial t^m}\right)\vartheta_{,i}\right] = \left(1+\sum_{m=1}^{M_2}\frac{\tau_q^m}{m!}\frac{\partial^m}{\partial t^m}\right)q_i. \tag{8}$$

Equation (8) is considered an extension to the generalized heat conduction equation devoid of a mechanical term.

Taking the divergence followed by the time derivative of the two sides of Eq. (8), we get

$$-k_t\left[\left(1+\sum_{m=1}^{M_1}\frac{\tau_\theta^m}{m!}\frac{\partial^m}{\partial t^m}\right)\frac{\partial}{\partial t} + \frac{\epsilon k_t^*}{k_t}\left(1+\sum_{m=1}^{M_1}\frac{\tau_\vartheta^m}{m!}\frac{\partial^m}{\partial t^m}\right)\right]\theta_{,ii} = \left(1+\sum_{m=1}^{M_2}\frac{\tau_q^m}{m!}\frac{\partial^m}{\partial t^m}\right)\frac{\partial}{\partial t}q_{i,i}, \tag{9}$$

or

$$-k_t L_1 \theta_{,ii} = L_2 \frac{\partial}{\partial t} q_{i,i}, \tag{10}$$

where L_1 and L_2 are higher-order time derivative differential operators

$$L_1 = \left(1 + \sum_{m=1}^{M_1} \frac{\tau_\theta^m}{m!} \frac{\partial^m}{\partial t^m}\right) \frac{\partial}{\partial t} + \frac{\epsilon k_t^*}{k_t} \left(1 + \sum_{m=1}^{M_1} \frac{\tau_\vartheta^m}{m!} \frac{\partial^m}{\partial t^m}\right), \quad L_2 = 1 + \sum_{m=1}^{M_2} \frac{\tau_q^m}{m!} \frac{\partial^m}{\partial t^m}, \tag{11}$$

replacing the energy equation, Eq. (2), with the above equation tends to

$$k_t L_1 \theta_{,ii} = L_2 \left(\rho_t c_t \ddot{\theta} + \gamma_t T_0 \ddot{e} - \dot{Q} \right). \tag{12}$$

Thus Eq. (12) represents the refined TPL generalized thermoelasticity theory, that will be used for this paper with the motion equilibrium equations without body force and the constitutive relations, given as

$$\mu_t u_{i,jj} + (\lambda_t + \mu_t) u_{j,ji} - \gamma_t \theta_{,i} = \rho_t \ddot{u}_i, \tag{13}$$

$$\sigma_{ij} = 2\mu_t e_{ij} + \delta_{ij} (\lambda_t e_{kk} - \gamma_t \theta), \tag{14}$$

where u_i are the component of the displacement, δ_{ij} the Kronecker delta function, and

$$e_{ij} = \frac{1}{2} \left(u_{i,j} + u_{j,i} \right). \tag{15}$$

From Eq. (12), one can obtain the following models:

- CTE model
  It appears by setting $\tau_\theta = \tau_q = \epsilon = 0$

$$k_t \theta_{,ii} = \rho_t c_t \dot{\theta} + \gamma_t T_0 \dot{e} - Q. \tag{16}$$

- G–N III model
  It appears by omitting all relaxation times, i.e., $\tau_\theta = \tau_\vartheta = \tau_q = 0$, $\epsilon = 1$

$$\left(k_t \frac{\partial}{\partial t} + k_t^* \right) \theta_{,ii} = \rho_t c_t \ddot{\theta} + \gamma_t T_0 \ddot{e} - \dot{Q}. \tag{17}$$

- SPL model
  This model will appear when $\tau_\theta = \epsilon = 0$ and $M_2 = 1$

$$k_t \theta_{,ii} = \left(1 + \tau_q \frac{\partial}{\partial t} \right) \left(\rho_t c_t \dot{\theta} + \gamma_t T_0 \dot{e} - Q \right). \tag{18}$$

- DPL model
  This model will be given by setting $\epsilon = 0$ and $M_1 = M_2 = 1$

$$k_t \left(1 + \tau_\theta \frac{\partial}{\partial t} \right) \theta_{,ii} = \left(1 + \tau_q \frac{\partial}{\partial t} \right) \left(\rho_t c_t \dot{\theta} + \gamma_t T_0 \dot{e} - Q \right). \tag{19}$$

- Simple TPL model
  Now, the simple TPL model is given by taking the first-order derivatives for each of three phase lags, i.e., $M_1 = M_2 = 1$ and $\epsilon = 1$

$$\left[k_t \left(1 + \tau_\theta \frac{\partial}{\partial t} \right) \frac{\partial}{\partial t} + k_t^* \left(1 + \tau_\vartheta \frac{\partial}{\partial t} \right) \right] \theta_{,ii} = \left(1 + \tau_q \frac{\partial}{\partial t} \right) \left(\rho_t c_t \ddot{\theta} + \gamma_t T_0 \ddot{e} - \dot{Q} \right). \tag{20}$$

All of the above models used the equations of motion and the constitutive relations which are given in Eqs. (13)-(15).

When studying the thermoelastic responses of biological tissue to thermal loads, researchers [43-45] often use a heat source term written as $Q = w_b \rho_b c_b (T_b - T) + Q_m + Q_L$. The first component refers to the heat exchange that occurs between the biological tissue and the blood, where T_b represents the temperature of the blood. Q_m represents the heat generated by metabolic processes in tissue cells [46], while Q_L refers to the external thermal load applied to

the tissue [47].

An inhomogeneous boundary condition replaces the external heat source Q_L. This substitution results in the setting Q_L equal to zero. The analysis in this study does not include the consideration of metabolic heat generation Q_m within the tissue and assumes that $T_b = T_0$. Therefore, the remaining source of volumetric heat in the system is given as

$$Q = -w_b \rho_b c_b \theta, \tag{21}$$

where w_b represents the rate at which blood flows through tissue and the symbol ρ_b refers to the density of blood, while c_b represents the specific heat capacity of the blood.

Due to the challenges of solving the complex equations of three-dimensional thermoelasticity, researchers often use a simplified one-dimensional approximation to investigate the properties of thermoelastic responses in biological tissue. This approximation is sufficient for understanding these responses without facing the computational difficulties associated with the full three-dimensional model.

Therefore, Eqs. (12)-(15) can be rewritten in the one-dimensional form

$$k_t L_1 \frac{\partial^2 \theta}{\partial x^2} = L_2 \left[\frac{\partial^2}{\partial t^2} \left(\rho_t c_t \theta + \gamma_t T_b \frac{\partial u}{\partial x} \right) + w_b \rho_b c_b \frac{\partial \theta}{\partial t} \right], \tag{22}$$

$$(\lambda_t + 2\mu_t) \frac{\partial^2 u}{\partial x^2} - \gamma_t \frac{\partial \theta}{\partial x} = \rho_t \frac{\partial^2 u}{\partial t^2}, \tag{23}$$

$$\sigma = (\lambda_t + 2\mu_t) e - \gamma_t \theta, \tag{24}$$

$$e = \frac{\partial u}{\partial x}, \tag{25}$$

where

$$L_1 = \sum_{m=0}^{M} \frac{\tau_\theta^m}{m!} \frac{\partial^{m+1}}{\partial t^{m+1}} + \frac{\epsilon k_t^*}{k_t} \sum_{m=0}^{M} \frac{\tau_\vartheta^m}{m!} \frac{\partial^m}{\partial t^m}, \quad L_2 = \sum_{m=0}^{M} \frac{\tau_q^m}{m!} \frac{\partial^m}{\partial t^m}. \tag{26}$$

3. Analytical solution

Let us take a look at the modified TPL model, which is depicted by Eqs. (22)-(24) and can be expressed as

$$\frac{\partial^2 u}{\partial x^2} - c_1 \frac{\partial \theta}{\partial x} = \frac{1}{C_P^2} \frac{\partial^2 u}{\partial t^2}, \tag{27}$$

$$C_T^2 \frac{\partial^2 \theta}{\partial x^2} = \left(w_b \rho_c + \frac{\partial}{\partial t} \right) \frac{\partial \theta}{\partial t} + \eta \frac{\partial^3 u}{\partial t^2 \partial x}, \tag{28}$$

$$\frac{\sigma}{\lambda_t + 2\mu_t} = \frac{\partial u}{\partial x} - c_1 \theta, \tag{29}$$

where

$$c_1 = \frac{\gamma_t}{\lambda_t + 2\mu_t}, \quad C_P^2 = \frac{\lambda_t + 2\mu_t}{\rho_t}, \quad C_T^2 = \frac{k_t L_1}{\rho_t c_t L_2}, \quad \rho_c = \frac{\rho_b c_b}{\rho_t c_t}, \quad \eta = \frac{\gamma_t T_b}{\rho_t c_t}. \tag{30}$$

Now, we will proceed to present the initial and boundary conditions of the problem. The initial conditions for the issue under consideration are assumed to be homogeneous, which can be described in the following manner

$$\theta(x,t)|_{t=0} = 0, \quad \left. \frac{\partial^n \theta(x,t)}{\partial t^n} \right|_{t=0} = 0, \quad u(x,t)|_{t=0} = \left. \frac{\partial^n u(x,t)}{\partial t^n} \right|_{t=0} = 0, \quad n \geq 1. \tag{31}$$

The biological tissue is not subjected to any forces on both its internal and external surfaces. Only the outer surface of the skin tissue experiences thermal loading, while the inner surface remains insulated with no heat transfer occurring between it and the surrounding tissue. Therefore, the boundary conditions of the biological tissue being studied are expressed as

$$\theta(0,t) = g(t), \quad \theta_x(L,t) = 0, \quad \sigma(0,t) = 0, \quad \sigma(L,t) = 0, \tag{32}$$

where $g(t)$ represents the thermal load function applied to the upper surface of the skin tissue at $x = 0$, as depicted in Fig. 1. Next, we assume that the tissue's plane $x = 0$ is exposed to the thermal shock as follows:

$$g(t) = \theta_0 \, H(t - \nu), \quad t \geq \nu, \tag{33}$$

where the parameter $\theta_0 > 0$ represents the strength of the thermal loading, which indicates how much heat is applied to the system. $H(*)$ is the Heaviside unit step function that accounts for the timing of the loading, and the parameter $\nu \geq 0$ is known as the thermal shock parameter.

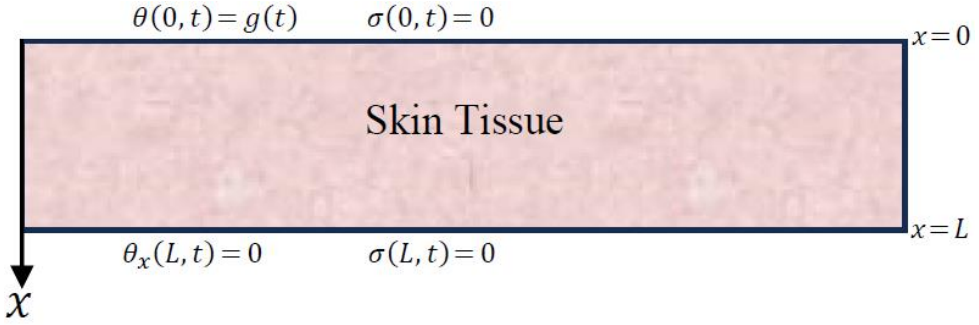

Fig. 1: A model of skin tissue that is one-dimensional and incorporates boundary conditions.

4. Laplace transforms

Utilizing the Laplace transform as explained in the context of

$$\bar{f}(x,s) = \int_0^\infty e^{-st} f(x,t) \, \mathrm{d}t. \tag{34}$$

By incorporating homogeneous initial conditions (31) and considering Eqs. (27)-(29) on both sides, we derive field equations in the Laplace transform domain as follows.

$$\left(\frac{d^2}{dx^2} - 2c_2\right)\bar{u} - c_1 \frac{d\bar{\theta}}{dx} = 0, \tag{35}$$

$$\left(\frac{d^2}{dx^2} - 2c_3\right)\bar{\theta} = 2c_4 \frac{d\bar{u}}{dx}, \tag{36}$$

$$\frac{\bar{\sigma}}{\lambda_t + 2\mu_t} = \frac{d\bar{u}}{dx} - c_1\bar{\theta}, \tag{37}$$

where

$$\begin{gathered} c_2 = \frac{s^2}{2\bar{C}_T^2}, \quad c_3 = \frac{(w_b \rho_c s + s^2)}{2\bar{C}_T^2}\bar{L}_2, \quad c_4 = \frac{\eta s^2}{2\bar{C}_T^2}\bar{L}_2, \\ \bar{C}_T^2 = \frac{k_t \bar{L}_1}{\rho_t c_t} = \frac{1}{\rho_t c_t}\left(k_t \sum_{m=0}^{M} \frac{\tau_\theta^m}{m!} s^{m+1} + k_t^* \sum_{m=0}^{M} \frac{\tau_\vartheta^m}{m!} s^m\right), \quad \bar{L}_2 = \sum_{m=0}^{M} \frac{\tau_q^m}{m!} s^m . \end{gathered} \tag{38}$$

The over bar symbol in this context signifies the Laplace transform, while the small letter s serves as an indicator for the Laplace parameter. To obtain the desired results, Equations (35) and (36) are solved within the context of the Laplace domain to obtain

$$\bar{\theta} = \sum_{i=1}^{2} \left(A_i \, e^{\xi_i x} + B_i \, e^{-\xi_i x}\right), \tag{39}$$

$$\bar{u} = \sum_{i=1}^{2} \beta_i \left(A_i \, e^{\xi_i x} - B_i \, e^{-\xi_i x}\right), \tag{40}$$

where A_i and B_i are constant coefficients that differ with respect to s, while the parameters ξ_i and β_i are specified as

$$\xi_1, \xi_2 = \sqrt{c_1 c_4 + c_2 + c_3 \pm \xi_0}, \quad \xi_0 = \sqrt{(c_1 c_4 + c_2)^2 + c_3[c_3 + 2(c_1 c_4 - c_2)]}, \tag{41}$$

$$\beta_i = \frac{\xi_i(\xi_i^2 - 2c_1 c_4 - 2c_3)}{4c_2 c_4}. \tag{42}$$

Furthermore, the dilatation in Eq. (25) is expressed in the Laplace domain as

$$\bar{e} = \sum_{i=1}^{2} \beta_i \xi_i \left(A_i\, e^{\xi_i x} + B_i\, e^{-\xi_i x}\right). \tag{43}$$

Moreover, the axial stress is obtained from Eq. (37) as

$$\bar{\sigma} = \sum_{i=1}^{2} \zeta_i \left(A_i\, e^{\xi_i x} + B_i\, e^{-\xi_i x}\right), \tag{44}$$

where

$$\zeta_i = (\lambda_t + 2\mu_t)(\beta_i \xi_i - c_1). \tag{45}$$

Within the domain of the Laplace transform, the boundary conditions (16) can be formulated as

$$\bar{\theta}(x,s)\big|_{x=0} = \frac{\theta_0 e^{-vs}}{s} = \bar{G}_s, \tag{46}$$

$$\bar{\theta_x}(x,s)\big|_{x=L} = 0, \quad \bar{\sigma}(x,s)|_{x=0,L} = 0. \tag{47}$$

By successfully solving the intricate arrangement of direct conditions, we are able to determine the values for the elusive parameters A_i and B_i. By imposing these boundary conditions on Eqs. (39) and (40), we arrive at

$$\begin{bmatrix} 1 & 1 & 1 & 1 \\ \xi_1 e^{\xi_1 L} & \xi_1 e^{-\xi_1 L} & \xi_2 e^{\xi_2 L} & \xi_2 e^{-\xi_2 L} \\ \zeta_1 & \zeta_1 & \zeta_2 & \zeta_2 \\ \zeta_1 e^{\xi_1 L} & \zeta_1 e^{-\xi_1 L} & \zeta_2 e^{\xi_2 L} & \zeta_2 e^{-\xi_2 L} \end{bmatrix} \begin{Bmatrix} A_1 \\ B_1 \\ A_2 \\ B_2 \end{Bmatrix} = \begin{Bmatrix} \bar{G}_s \\ 0 \\ 0 \\ 0 \end{Bmatrix}. \tag{48}$$

By solving the system of linear equations mentioned previously, we can find the values of the parameters that lead to the desired solutions in the Laplace transform domain

$$A_1 = \frac{1}{\Delta}\zeta_2 \bar{G}_s \left(\Lambda_1 e^{(\xi_1+\xi_2)L} - \Lambda_2 e^{(\xi_1-\xi_2)L} - 2\zeta_1 \xi_2 e^{2\xi_1 L}\right), \tag{49}$$

$$B_1 = -\frac{1}{\Delta}\zeta_2 \bar{G}_s \left(\Lambda_1 e^{(3\xi_1-\xi_2)L} - \Lambda_2 e^{(3\xi_1+\xi_2)L} - 2\zeta_1 \xi_2 e^{2\xi_1 L}\right), \tag{50}$$

$$A_2 = \frac{1}{\Delta}\zeta_1 \bar{G}_s \left(\Lambda_1 e^{(3\xi_1-\xi_2)L} + \Lambda_2 e^{(\xi_1-\xi_2)L} - 2\xi_1 \zeta_2 e^{2\xi_1 L}\right), \tag{51}$$

$$B_2 = -\frac{1}{\Delta}\zeta_1 \bar{G}_s \left(\Lambda_1 e^{(\xi_1+\xi_2)L} + \Lambda_2 e^{(3\xi_1+\xi_2)L} - 2\xi_1 \zeta_2 e^{2\xi_1 L}\right), \tag{52}$$

where

$$\Lambda_1, \Lambda_2 = \xi_1 \zeta_2 \pm \xi_2 \zeta_1, \tag{53}$$

$$\Delta = (\zeta_1 - \zeta_2)\left[\Lambda_1 \left(e^{(3\xi_1-\xi_2)L} - e^{(\xi_1+\xi_2)L}\right) + \Lambda_2 \left(e^{(\xi_1-\xi_2)L} - e^{(3\xi_1+\xi_2)L}\right)\right]. \tag{54}$$

The issue in the transformation domain has been effectively addressed. However, due to the formidable complexity of Equations (39) and (40), achieving an analytical inverse transform in the time domain becomes a highly intricate

and challenging task. Accordingly, we will make use of the Laplace transform numerical inversion method to examine the behaviors of field variables in the time domain. To obtain numerical results in the physical domain, we utilize the Riemann-sum approximation method as a computational approach for estimation. In this method, the conversion of any function $\bar{f}(x,s)$ from the Laplace transform space to the physical domain $f(x,t)$ is achieved by employing a well-known equation [48]

$$f(x,t)=\frac{e^{\varrho t}}{t}\left[\frac{1}{2}\mathrm{Re}\{\bar{f}(x,\varrho)\}+\mathrm{Re}\left\{\sum_{n=0}^{N}\left(\bar{f}\left(x,\varrho+\frac{n\pi I}{t}\right)(-1)^n\right)\right\}\right]. \tag{55}$$

The symbol Re represents the real part of a function, while I denotes the imaginary unit ($\mathrm{I}=\sqrt{-1}$). Several numerical experiments have demonstrated that the value of ϱ approximately follows the relation $\varrho t\approx 4.7$ to achieve rapid convergence.

5. Numerical findings and discussions

In the subsequent part, we present a comprehensive overview and analysis of the numerical findings for all variables concerning skin tissue. The influence of the thermal shock parameter and phase lag times is investigated with various generalized thermoelastic theories, with a focus on understanding their effects on both thermal and elastic responses. Table 1 presents a compilation of the thermophysical characteristics of blood and biological tissue, as documented in references [49-51]. To simulate the conditions, a temperature load of $\theta_0=80$ K is imposed on the skin surface, with the skin tissue having a thickness of $L=1$ mm. The quantities of temperature (θ), displacement (u), volumetric strain (u), and axial stress (σ) are determined using Eq. (55). The numerical results are then analyzed extensively and presented in Figures 2-17.

Table 1: Key material characteristics of skin tissue for bioheat transfer analysis.

Parameter	Value	Uint
λ_t	8.27×10^8	kg/(m s^2)
μ_t	3.446×10^7	kg/(m s^2)
ρ_t	1190	kg/m^3
c_t	3600	J/(K kg)
k_t	0.235	W/(m K)
ρ_b	1060	kg/m^3
c_b	3770	J/(K kg)
α_t	1×10^{-4}	(1/K)
T_b	310	K
w_b	1.87×10^3	$1/s$

5.1. Contrasting the refined TPL model with previous generalized theories

Figures 2-5 show the field quantities that can be gotten from different coupling theorems when the fixed relaxation times at time $t=4$ are $\tau_\vartheta=0.09$, $\tau_\theta=0.29$, and $\tau_q=0.69$.

Figure 2 displays a comparison of different theories, showing how temperature (θ) is distributed across the thickness of the skin tissue. The temperature exhibits a clear inverse relationship with x in the CTE, G–N III, DPL, and simple TPL generalized thermoelastic theories. As x increases, the temperature decreases accordingly. The SPL and refined TPL thermoelastic theories both produce responses that appear different from one another. Along with the skin tissue thickness, the temperature vibrates. Another obvious difference in thermal response is that the refined TPL model predicts the highest temperature than other models at $x=0.058$, while the SPL model predicts the lowest temperature at $x=0.18$.

In Fig. 3, the displacement distributions (u) across the thickness of the skin tissue are depicted for different theories. The displacement shows a direct increase with x in all cases. However, for CTE, G–N III, DPL, and simple TPL generalized theories, there is an additional displacement along the x direction due to thermal expansion. On the other hand, refined TPL and SPL models show slight oscillations along the thickness of the skin tissue after an initial increase with x.

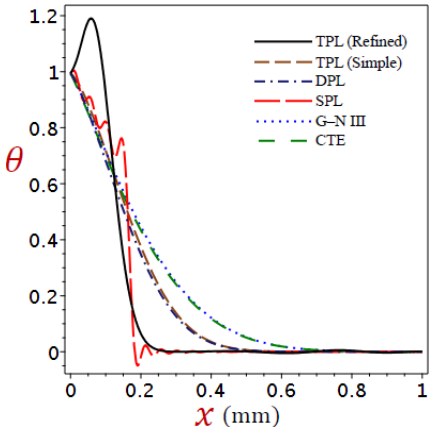

Fig. 2: Exploring the differences in temperature variation (θ) across skin tissue by considering multiple theories.

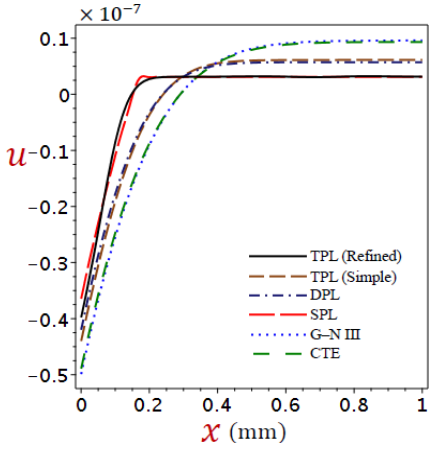

Fig. 3: Exploring the differences in displacement variation (u) across skin tissue by considering multiple theories.

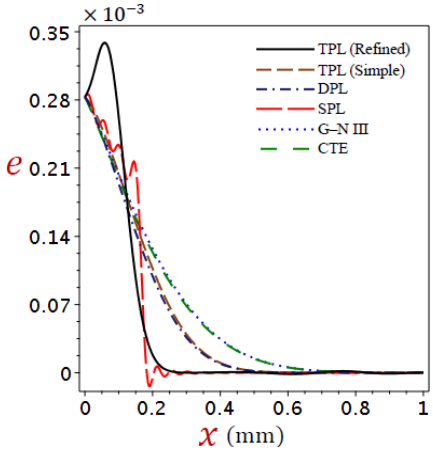

Fig. 4: Exploring the differences in dilatation variation (e) across skin tissue by considering multiple theories.

Figure 4 illustrates the different dilatation distributions (e) across the skin tissue resulting from the application of various theories. In the CTE, G–N III, DPL, and simple TPL generalized thermoelastic theories, there is a clear inverse relationship between dilatation and x. As x increases, the dilatation decreases accordingly. However, both SPL and refined TPL thermoelastic theories exhibit distinct responses. The dilatation oscillates along with the thickness of the skin tissue in these models. Additionally, at $x = 0.058$, the refined TPL model predicts higher dilatation compared to

other models, while at $x = 0.18$, the SPL model predicts lower dilatation than other models.

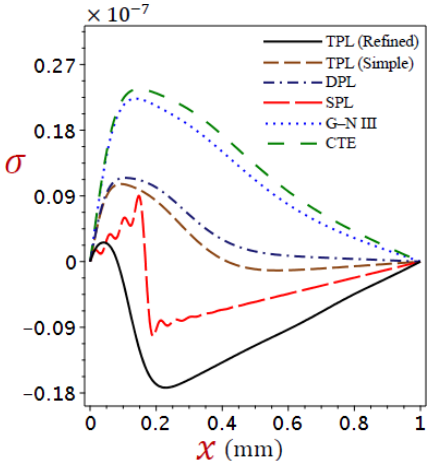

Fig. 5: Exploring the differences in stress variation (σ) across skin tissue by considering multiple theories.

Figure 5 shows how various theories predict variations in stress distribution (σ) across the thickness of the skin tissue. The stress distribution in the skin tissue is characterized by zero values at the boundary plane $x = 0$ and a gradual decrease to zero as we move towards the other side of the tissue, $x = L$, which adherence to mechanical boundary conditions on both sides suggests. The stress is no longer increasing directly as x increases, and there is a maximum value for each of the generalized thermoelastic models. Furthermore, in the SPL theory, it is observed that the stress curve exhibits a distribution that is different from the rest; the pressure vibrates along the depth of the tissue. The stresses obtained from the refined TPL generalized thermoelastic model are the lowest among all the models considered.

5.2. The influence of the thermal shock parameter

Figures 6-9 show the temperature, displacement, dilatation, and stress distributions for the G–N III, simple TPL, and refined TPL models for different values of the thermal shock parameter (v). Specifically, $v = 3.48$, 3.54, 3.60, and 3.66 with $t = 4$ are investigated to understand their effects on these distributions.

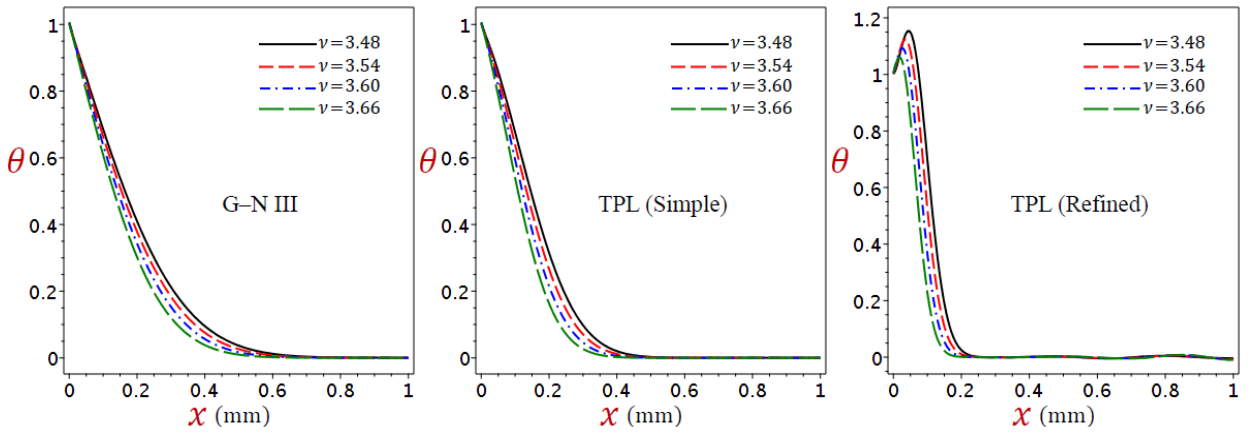

Fig. 6: Temperature profiles (θ) across the skin tissue with different values of the thermal shock parameter.

Once again, Fig. 6 demonstrates that the temperature distribution (θ) decreases directly across the skin tissue for both the G–N III and simple TPL generalized thermoelastic models. However, there is a distinct difference in how θ behaves concerning the refined TPL generalized thermoelastic model. Along with the skin tissue thickness, the temperature vibrates; generally, as v increases, θ exhibits a decreasing trend.

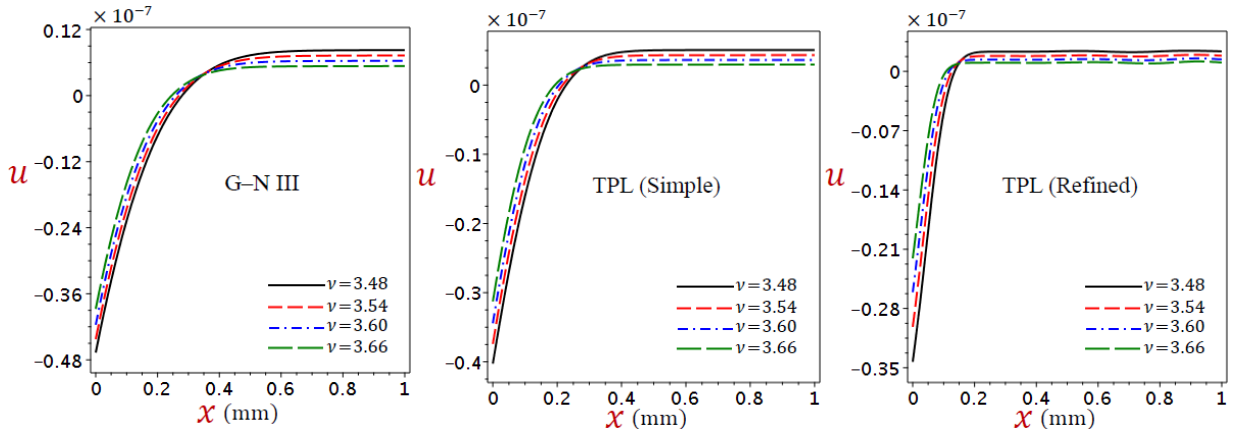

Fig. 7: Displacement profiles (u) across the skin tissue with different values of the thermal shock parameter.

In Fig. 7, the variations in displacement (u) across the thickness of the skin tissue are depicted for G–N III, simple TPL, and refined TPL models using different values of the thermal shock parameter. The displacements are equal at $x = 0.35$, 0.27, and 0.15 for the G–N III, simple TPL, and refined TPL models, respectively. Before reaching these positions, the displacement shows an increasing trend as ν increases. Conversely, after passing these positions, the displacement exhibits a decreasing pattern as ν increases. It is interesting to see that the displacement due to the refined theory oscillates after $x = 0.15$.

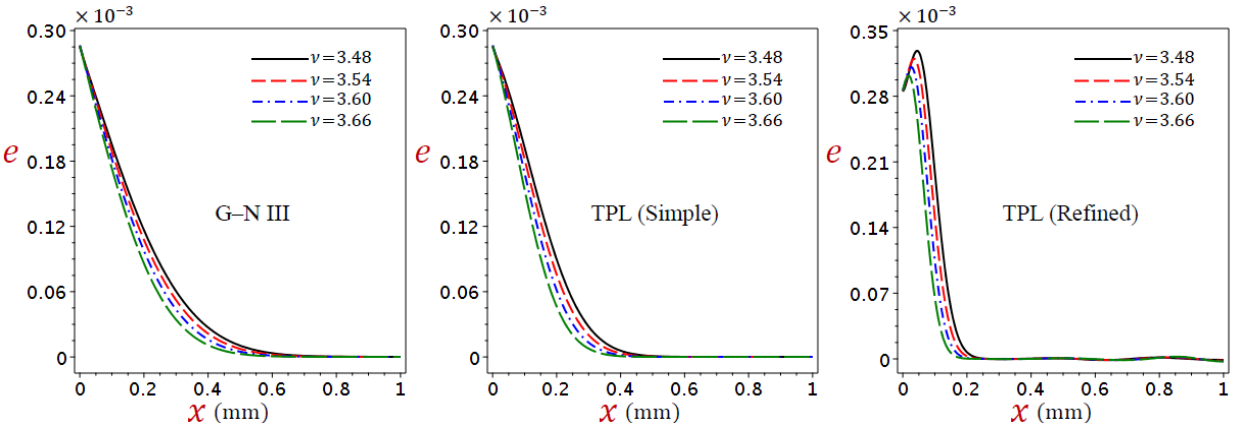

Fig. 8: Dilatation profiles (e) across the skin tissue with different values of the thermal shock parameter.

Figure 8 once again confirms that the dilatation distribution (e) decreases directly across the skin tissue in both the G–N III and simple TPL generalized thermoelastic models. However, there is a clear distinction in how e behaves with the refined TPL generalized thermoelastic model. In addition to varying with skin tissue thickness, e also exhibits oscillations; generally, as ν increases, there is a decreasing trend observed for e.

In Figure 9, the fluctuations in stress (σ) across the thickness of the skin tissue are presented for G–N III, simple TPL, and refined TPL models using various values of thermal shock parameters. The stress at the boundaries of the skin tissue is effectively nullified, in agreement with the mechanical boundary conditions imposed on both surfaces. We have a different stress curve shape in each model, noting that the refined TPL generalized thermoelastic model exhibits the lowest stress magnitudes, while the G–N III thermoelastic model shows the highest stress levels obtained. In general, the stress magnitude exhibits a positive correlation with the thermal shock parameter, indicating that higher values of the parameter result in increased stress levels.

5.3. The role of the thermal relaxation times

In TPL thermoelasticity, relaxation times play a crucial role in determining the thermal characteristics of organic tissue. Figures 10-13 present graphical representations of how temperature, displacement, dilatation, and stress for refined TPL vary under different phase lags while keeping the thermal shock parameter constant at $\nu = 3.4$ and time $t = 4$. The graph showcases three scenarios:

- Different values of τ_q with fixed values of $\tau_\vartheta = 0.09$ and $\tau_\theta = 0.28$.
- Different values of τ_θ with fixed values of $\tau_\theta = 0.09$ and $\tau_q = 0.76$.
- Different values of τ_ϑ with fixed values of $\tau_\theta = 0.28$ and $\tau_q = 0.76$.

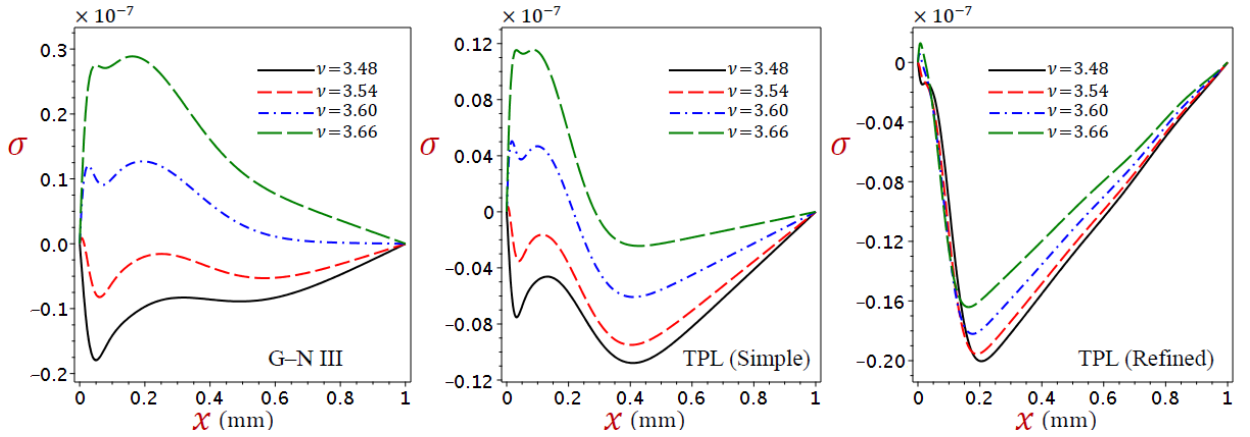

Fig. 9: Stress profiles (σ) across the skin tissue with different values of the thermal shock parameter.

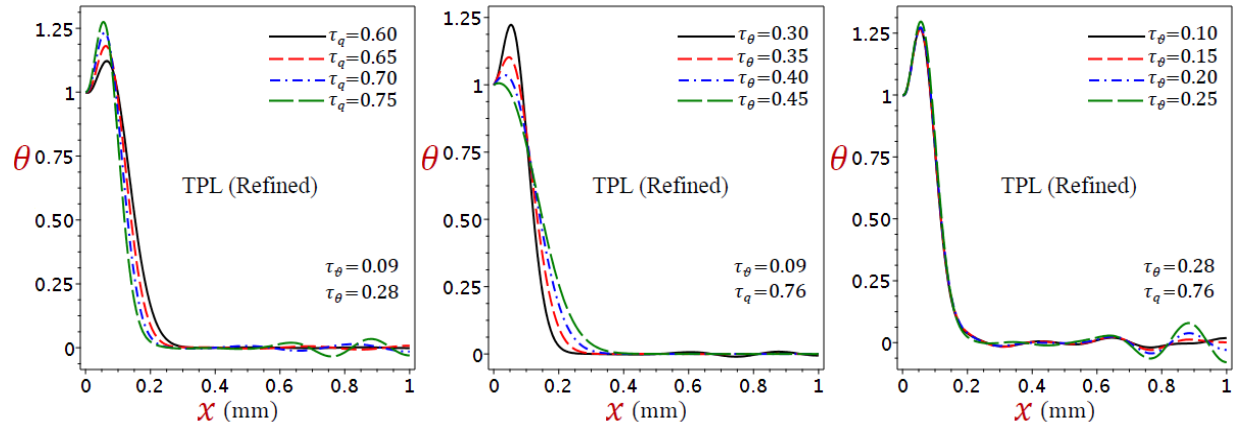

Fig. 10: Temperature (θ) distributions for the refined TPL model under (a) different τ_q (b) different τ_θ (c) different τ_ϑ.

In Fig. 10, the temperature variations (θ) resulting from the refined TPL model are depicted under three different scenarios. In Fig. 10a, the effect τ_q is being studied, which represents a lag phenomenon in the heat flux, indicating that thermal energy does not transfer instantaneously. Up until $x = 0.083$, an increase in τ_q causes the temperature to rise. However, beyond $x = 0.083$, an increase in τ_q leads to a decrease in temperature. The temperature exhibits oscillations in conjunction with the thickness of the skin tissue. Additionally, as τ_q increases, the amplitude of these temperature waves also increases.

Quite the opposite happens in Fig. 10b: when x is less than 0.104, an increase in τ_θ results in a temperature drop. Conversely, when x is greater than 0.104, an increase in τ_θ leads to an increase in temperature. Furthermore, with an increase in τ_θ, the amplitude of temperature oscillations diminishes.

In a similar vein, Fig. 10c exhibits the temperature profiles along the depth direction under different phase lag times of the thermal displacement gradient. Once again, the temperature in the biological tissue shows oscillations that are linked to the thickness of the skin tissue. Moreover, as τ_ϑ increases, these temperature waves become more pronounced with larger amplitudes. In general, as τ_ϑ increases, there is a corresponding increase in temperature.

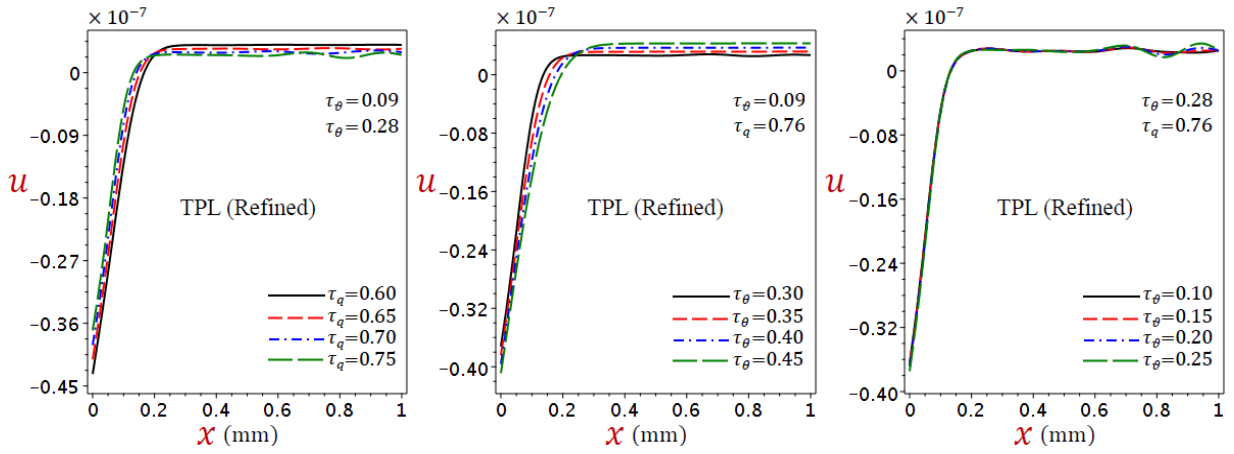

Fig. 11: Displacement (u) distributions for the refined TPL model under (a) different τ_q (b) different τ_θ (c) different τ_ϑ.

Figure 11 illustrates the variations in displacement (u) resulting from the refined TPL model across three different scenarios. Fig. 10a focuses on analyzing the effect of τ_q on the system. At $x = 0.18$, the displacements are almost equal. However, before this position, the displacement increases with an increase in τ_q and decreases vice versa after this point. Additionally, beyond $x = 0.18$, the displacement exhibits oscillations according to the refined theory, and as τ_q increases further, these oscillations have larger amplitudes.

On the contrary, Fig. 11b demonstrates a contrasting behavior: At $x = 0.285$, the displacements are almost equal. However, before this position, the displacement decreases as τ_θ increases, and vice versa after this point. Furthermore, beyond $x = 0.285$, according to the refined theory, there are oscillations observed in displacement where amplitudes decrease as τ_θ increases further.

Continuing similarly, Fig. 11c presents the displacement profiles along the depth direction for varying phase lag times of the thermal displacement gradient. Once more, the displacement within the biological tissue exhibits oscillations that are correlated with the thickness of the skin tissue. Furthermore, as τ_ϑ increases, these displacement waves display larger amplitudes. Overall, there is a decrease in displacement as τ_ϑ increases.

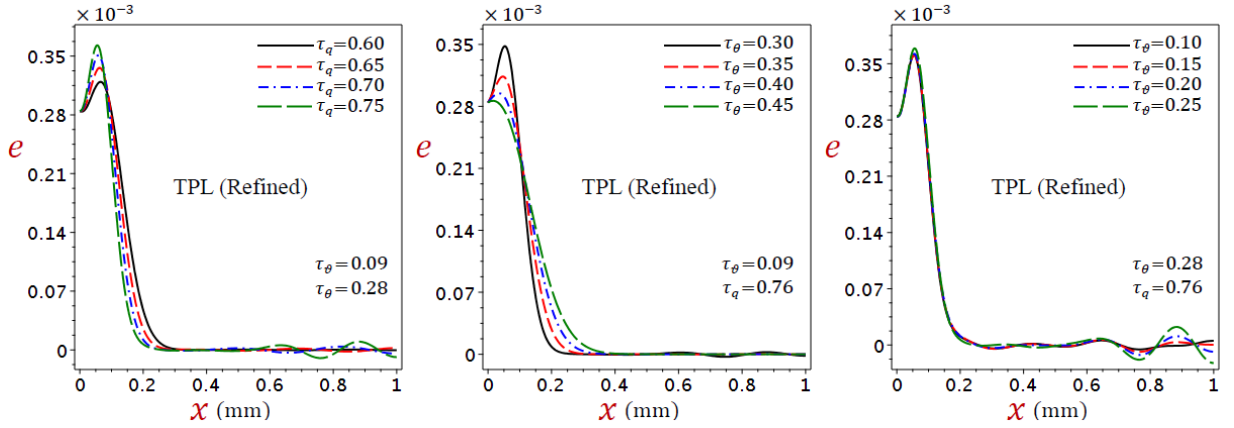

Fig. 12: Dilatation (e) distributions for the refined TPL model under (a) different τ_q (b) different τ_θ (c) different τ_ϑ.

Figure 12 illustrates the variations in dilatation (e) predicted by the refined TPL model across three different scenarios. In Fig. 12a, the influence of τ_q is examined on dilatation. Until $x = 0.083$, an increase in τ_q results in a rise in dilatation. However, beyond $x = 0.083$, increasing τ_q leads to a decrease in dilatation instead. The dilatation demonstrates oscillations that correspond with the thickness of the skin tissue as well; furthermore, as τ_q increases further, these oscillations exhibit larger amplitudes.

Figure 12b presents a contrasting pattern: for x values less than 0.104, an increase in τ_θ causes a decrease in dilatation. Conversely, for x values greater than 0.104, an increase in τ_θ leads to an increase in dilatation instead. Additionally, as τ_θ increases further, the amplitude of dilatation oscillations diminishes.

Similarly, Fig. 12c demonstrates the expansion patterns along the depth axis for various phase lag times of the

thermal displacement gradient. Once again, the dilatation in biological tissue exhibits oscillatory patterns that are correlated with the thickness of the skin tissue. Furthermore, as τ_ϑ increases, these waves of dilatation become more prominent with larger amplitudes. In general, an increase in τ_ϑ corresponds to an increase in overall dilatation within the tissue.

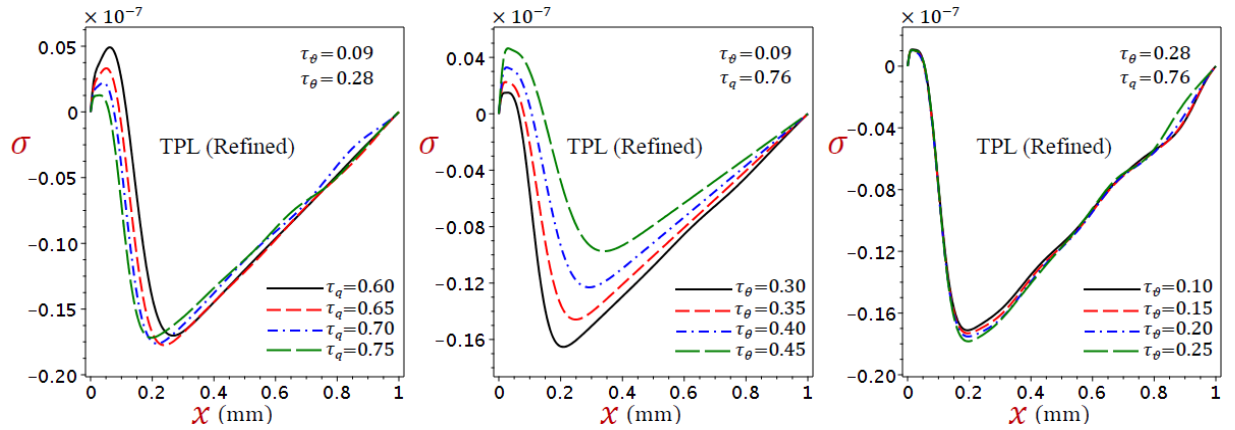

Fig. 13: Stress (σ) distributions for the refined TPL model under (a) different τ_q (b) different τ_θ (c) different τ_ϑ.

Figure 13 displays the stress variations (σ) across the thickness of the skin tissue, presenting three different scenarios based on the refined TPL model. The stress becomes zero at the edges of the skin tissue, aligning with the mechanical boundary conditions on both surfaces. Figure 13b shows that the refined TPL generalized thermoelastic model shows a uniform rise in stress as the relaxation time of the temperature gradient τ_θ goes up. However, this uniform increase does not occur when considering the relaxation times of both the heat flux τ_q and the thermal displacement gradient τ_ϑ, as shown in Figs. 13a,c. These findings suggest that the refined model exhibits distinct behaviors when subjected to changes in relaxation times.

5.4. The impact of the times and blood perfusion rate

Figures 14(a–f) illustrate the variations in temperature (θ) and displacement (u)distributions across different time points for the G–N III, simple TPL, and refined TPL models. Specifically, we examine time intervals $t = 4.4$, 4.5, 4.6, and 4.7 with a thermal shock parameter $\nu = 3.95$ to analyze their impact on these distributions.

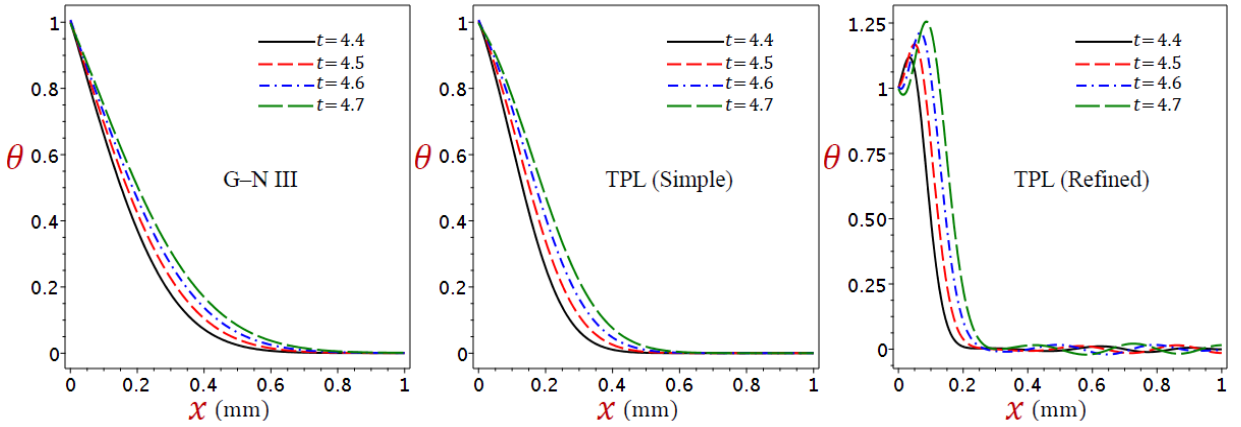

(a) (b) (c)

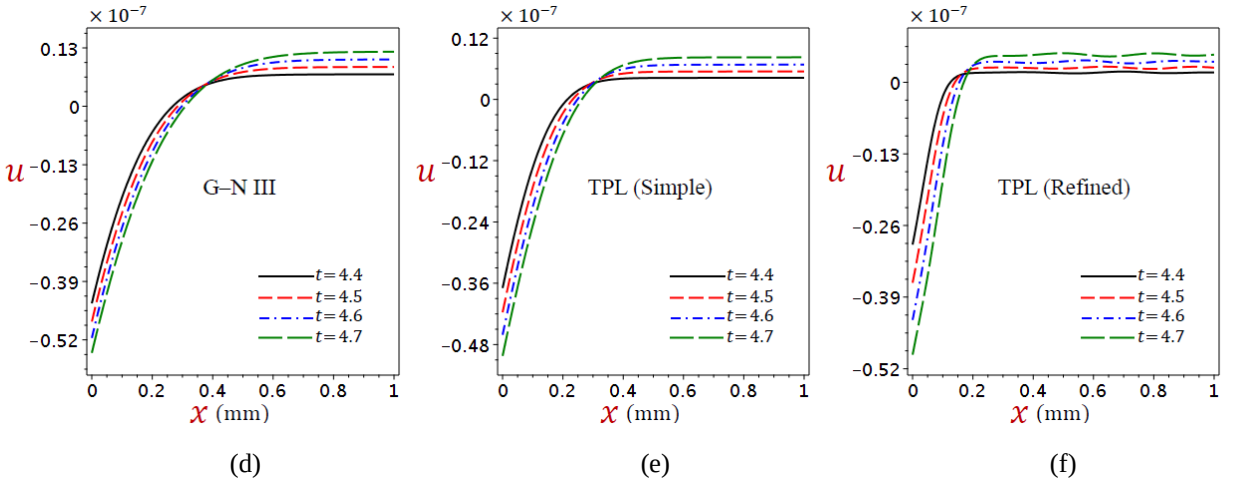

Fig. 14: Distribution of temperature (θ) and displacement (u) across skin tissue at various time points (t) for G–N III, simple TPL, and refined TPL.

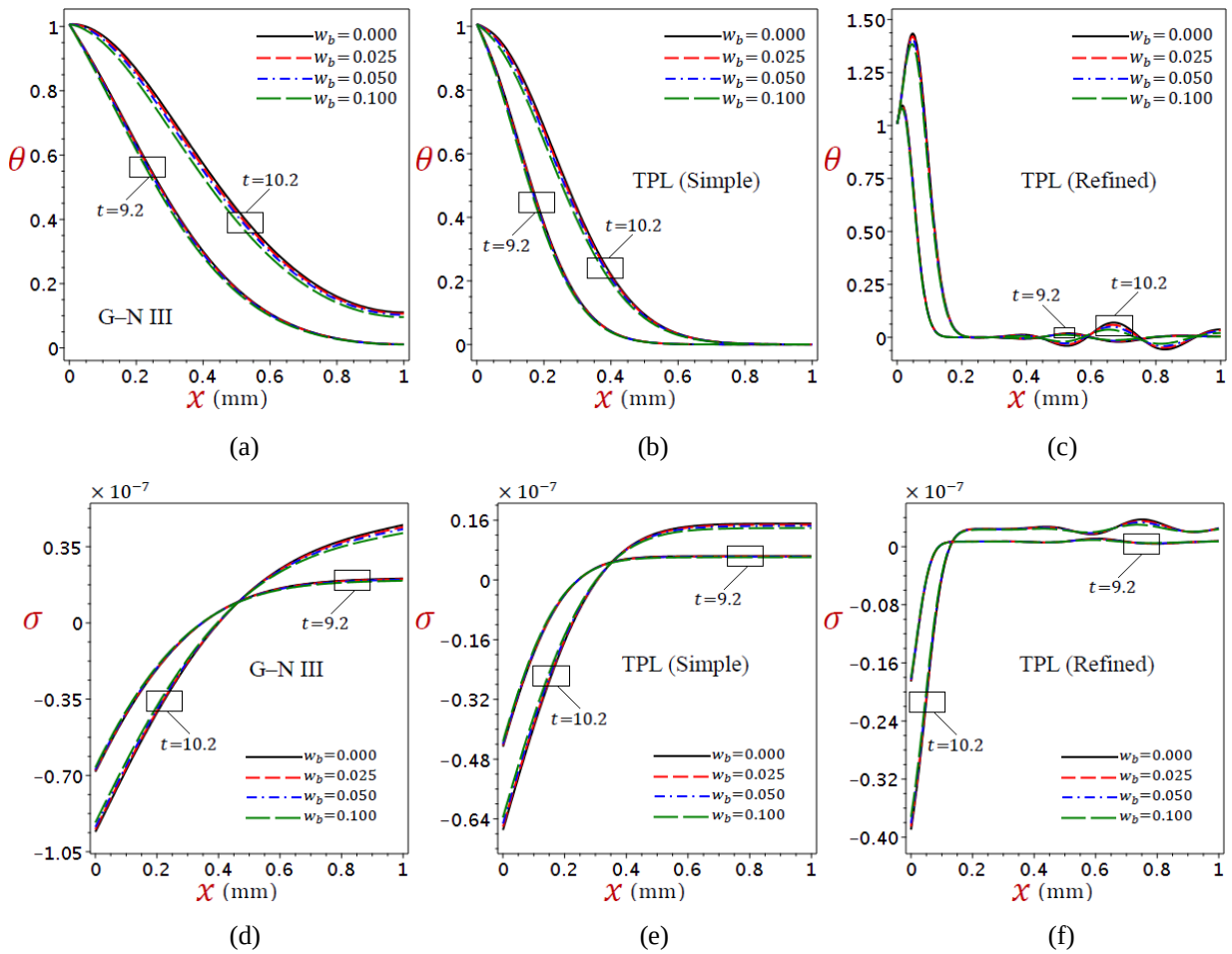

Fig. 15: Distribution of temperature (θ) and displacement (u) across skin tissue for the G–N III, simple TPL, and refined TPL models at different values of blood perfusion rate (w_b).

Figures 14a-c show that the temperature drops straight across the skin tissue in both the G–N III and simple TPL generalized thermoelastic models. However, there is a noticeable distinction in how θ behaves when considering the refined TPL generalized thermoelastic model. In addition to vibrating for skin tissue thickness, temperature waves

also exhibit an increase in amplitude as time progresses. Overall, these findings suggest that as time elapses, temperatures rise while decreasing with increasing tissue depth.

Figures 14d-f illustrate the variations in displacement (u) across the thickness of the skin tissue for G–N III, simple TPL, and refined TPL models at different time points. At $x = 0.384$, 0.31, and 0.187 positions within the tissue, the displacements are nearly equal for the G–N III, simple TPL, and refined TPL models, respectively.

Before reaching the positions mentioned above, the displacement demonstrates a decreasing trend as time increases. However, on passing these positions, the displacement exhibits an increasing pattern with increasing time. It is intriguing to observe that after $x = 0.187$, the displacement resulting from refined theory oscillates.

To illustrate the impact of blood perfusion rate (w_b), Figures 18a-f showcase the temperature and displacement distributions in the G–N III, simple TPL, and refined TPL models at two distinct time points: $t = 9.2$ and $t = 10.2$. The thermal relaxation times are $\tau_\vartheta = 0.1$, $\tau_\theta = 1.3$, and $\tau_\theta = 5.4$, while $\nu = 8$ for all models considered in this analysis.

In Figs. 15a-c, it is observed that at time $t = 9.2$, the effect of the change in blood perfusion rate (w_b) seems to be relatively weak. However, when considering a longer time $(t = 10.2)$, the difference becomes more pronounced. Specifically, an increase in the rate of blood perfusion results in lower temperature values.

In the same way, in displacement (Figs. 15d-f), changing the blood perfusion rate (w_b) doesn't seem to have much of an effect at $t = 9.2$, but when we look at $t = 10.2$, the difference is much clearer.

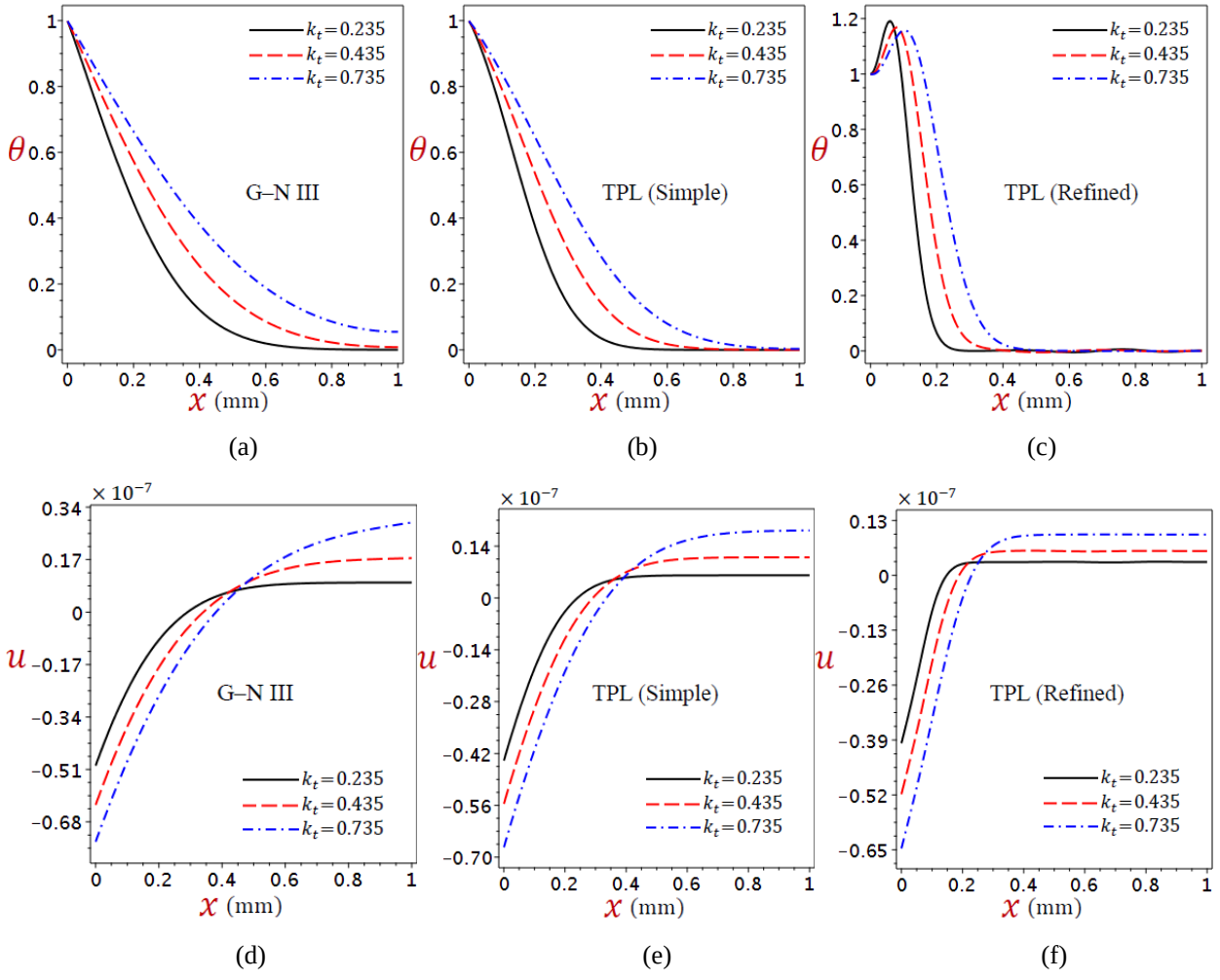

Fig. 16: Distributions of temperature (θ) and displacement (u) across skin tissue for the G–N III, simple TPL, and refined TPL models at numerous values of heat conductivity (k_t).

5.5. The significance of thermal conductivity and its rate

The thermal conductivity k_t of a tissue is an inherent property that measures its ability to conduct heat, while the rate of thermal conductivity k_t^* refers to how quickly heat is conducted through the tissue. These two factors play a

significant role in understanding and analyzing thermoelastic behavior in organic tissues.

Figures 16a-f depict the temperature distribution (θ) and displacement distribution (u) across the skin tissue using different values of heat conductivity k_t. In contrast, Figs. 17a-f illustrate the same distributions but with varying rates of thermal conductivity k_t^*, within the context of G–N III, simple TPL, and refined TPL models.

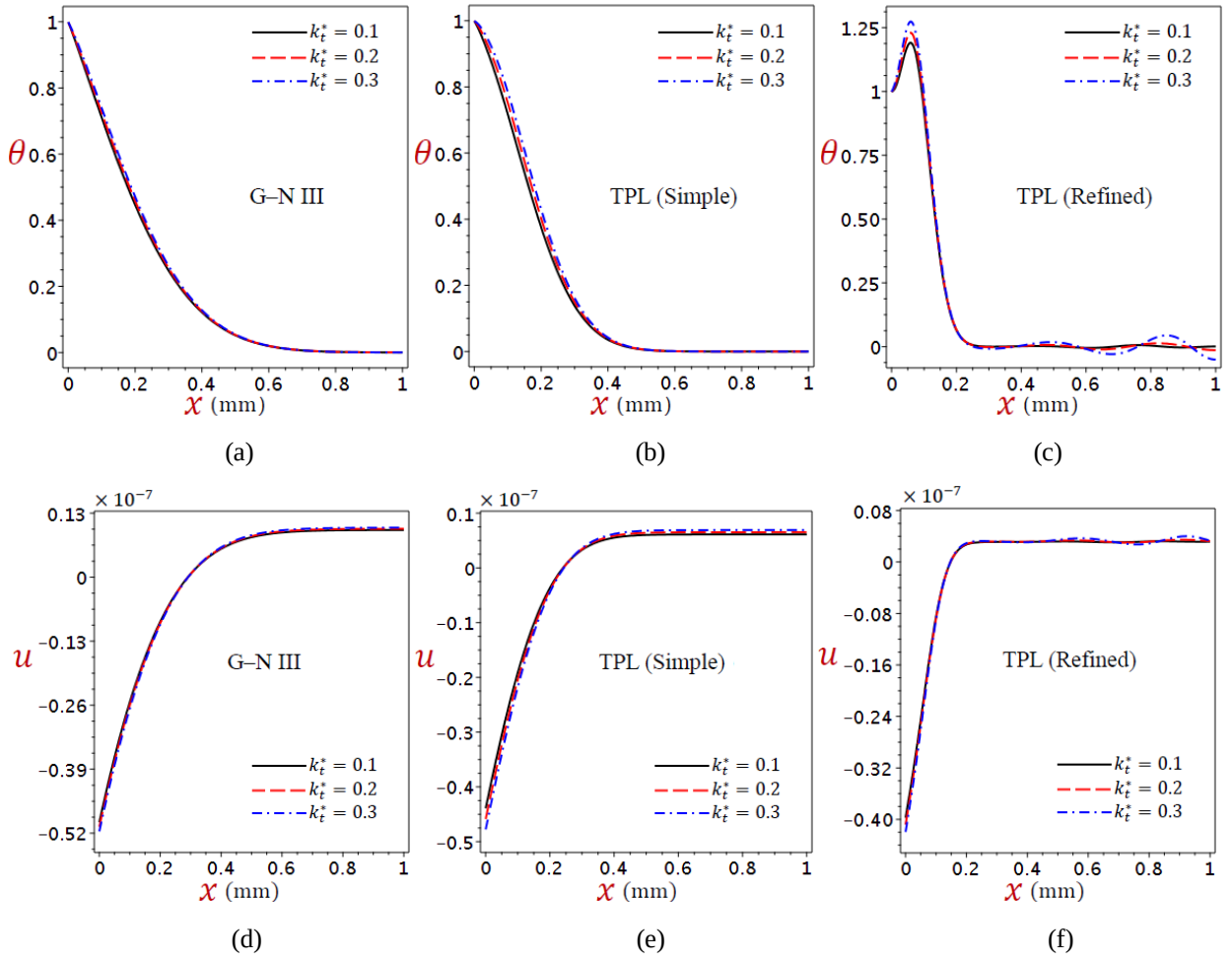

Fig. 17: Distributions of temperature (θ) and displacement (u) across skin tissue for the G–N III, simple TPL, and refined TPL models at numerous values of heat conductivity (k_t^*).

When considering the impact on temperature distribution, it is evident that thermal conductivity has a greater effect compared to the rate of thermal conduction. Increasing values for both k_t and k_t^* lead to elevated temperatures within the tissue. According to the refined theory, there are oscillations in temperature with the thickness of the skin tissue, where amplitudes increase as k_t^* increases further, and the opposite happens concerning k_t.

Similarly, when considering the impact on displacement distribution, it becomes evident that thermal conductivity has a greater influence compared to the rate of thermal conduction. Furthermore, as depicted in Figs. 17d-f, we observe that before reaching $x = 0.3$, 0.24, and 0.146 positions for the G–N III, simple TPL, and refined TPL models, respectively, an increase in k_t^* leads to a decrease in displacement (u). However, after surpassing these positions along the thickness direction x, there is an opposite trend where increasing k_t^* results in an increase in displacement (u). This behavior does not hold for changes in k_t in Figs. 16d-f.

6. Conclusions

In this study, we propose a newly utilized thermoelasticity model based on a higher-order time derivative of the TPL approach. We apply this model to analyze the thermal conduction equation in skin tissue subjected to a thermal shock. The refined TPL thermoelasticity model offers a distinct perspective by considering the influence of multiple time derivatives on thermo-mechanical phenomena. This sets it apart from conventional generalized thermoelasticity theories, making it a valuable tool for studying complex thermal behavior in materials. We considered a one-

dimensional skin tissue with a thin profile, where the outer surface was free from traction and the inner surface experienced no change in temperature or traction. The proposed model's governing equations are derived from the principles of generalized thermoelasticity theory. To analyze the data, Laplace transform techniques were employed. Subsequently, the Tzuo method was utilized to invert the transformed data and obtain numerical results in the time domain. This methodology allowed for a comprehensive examination of various quantities of interest within our system and facilitated accurate calculations for further analysis. The previously established generalized thermoelastic theories can be derived as special cases from the model presented in this study. A comprehensive comparison was conducted between the refined TPL generalized thermoelastic model and existing generalized thermoelastic theories. Both the analytical and numerical analyses of the governing equations reveal a substantial impact from various factors, including the thermal shock parameter, relaxation times, blood perfusion rate, heat conductivity, rate of heat conductivity, and time parameters. These findings highlight the importance of considering these variables when studying thermoelastic behavior in skin tissue. This investigation is crucial for addressing skin tissue problems, as the material parameters in such cases are temperature-dependent. Ultimately, the proposed model can be utilized in various bioheat transfer applications.

References

[1] K. Mitra, S. Kumar, A. Vedevarz, M. K. Moallemi, Experimental Evidence of Hyperbolic Heat Conduction in Processed Meat, *Journal of Heat Transfer*, Vol. 117, No. 3, pp. 568-573, 1995.

[2] C. Cattaneo, A Form of Heat-Conduction Equations Which Eliminates the Paradox of Instantaneous Propagation, *Comptes Rendus*, Vol. 247, pp. 431, 1958, 1958.

[3] P. Vernotte, Les paradoxes de la theorie continue de l'equation de la chaleur, *Compt. Rendu*, Vol. 246, pp. 3154-3155, 1958, 1958.

[4] D. Y. Tzou, The generalized lagging response in small-scale and high-rate heating, *International Journal of Heat and Mass Transfer*, Vol. 38, No. 17, pp. 3231-3240, 1995/11/01/, 1995.

[5] S. R. Choudhuri, On a thermoelastic three-phase-lag model, *Journal of Thermal Stresses*, Vol. 30, No. 3, pp. 231-238, 2007.

[6] F. Xu, K. A. Seffen, T. J. Lu, Non-Fourier analysis of skin biothermomechanics, *International Journal of Heat and Mass Transfer*, Vol. 51, No. 9, pp. 2237-2259, 2008/05/01/, 2008.

[7] M. A. Biot, Thermoelasticity and irreversible thermodynamics, *Journal of applied physics*, Vol. 27, No. 3, pp. 240-253, 1956.

[8] H. W. Lord, Y. Shulman, A generalized dynamical theory of thermoelasticity, *Journal of the Mechanics and Physics of Solids*, Vol. 15, No. 5, pp. 299-309, 1967.

[9] A. E. Green, K. Lindsay, Thermoelasticity, *Journal of elasticity*, Vol. 2, No. 1, pp. 1-7, 1972.

[10] R. B. Hetnarski, J. Ignaczak, Nonclassical dynamical thermoelasticity, *International Journal of Solids and Structures*, Vol. 37, pp. 215-224, 01/31, 2000.

[11] A. E. Green, P. M. Naghdi, ON UNDAMPED HEAT WAVES IN AN ELASTIC SOLID, *Journal of Thermal Stresses*, Vol. 15, No. 2, pp. 253-264, 1992/04/01, 1992.

[12] A. Green, P. Naghdi, Thermoelasticity without energy dissipation, *Journal of elasticity*, Vol. 31, No. 3, pp. 189-208, 1993.

[13] M. Marin, A. Hobiny, I. Abbas, Finite Element Analysis of Nonlinear Bioheat Model in Skin Tissue Due to External Thermal Sources, *Mathematics*, Vol. 9, No. 13, pp. 1459, 2021.

[14] E. A. N. Al-Lehaibi, Mathematical Modelling with the Exact Solution of Three Different Bioheat Conduction Models of a Skin Tissue Shocked by Thermoelectrical Effect, *International Journal of Biomaterials*, Vol. 2023, pp. 3863773, 2023/07/17, 2023.

[15] S. K. Sharma, D. Kumar, A Study on Non-Linear DPL Model for Describing Heat Transfer in Skin Tissue during Hyperthermia Treatment, *Entropy*, Vol. 22, No. 4, pp. 481, 2020.

[16] H. M. Youssef, N. A. Alghamdi, The exact analytical solution of the dual-phase-lag two-temperature bioheat transfer of a skin tissue subjected to constant heat flux, *Scientific Reports*, Vol. 10, No. 1, pp. 15946, 2020/09/29, 2020.

[17] Q. Zhang, Y. Sun, J. Yang, Bio-heat response of skin tissue based on three-phase-lag model, *Scientific Reports*, Vol. 10, No. 1, pp. 16421, 2020.

[18] A. Hobiny, F. Alzahrani, I. Abbas, Analytical Estimation of Temperature in Living Tissues Using the TPL Bioheat Model with Experimental Verification, *Mathematics*, Vol. 8, pp. 1188, 07/19, 2020.

[19] R. Verma, S. Kumar, Numerical study on heat distribution in biological tissues based on three-phase lag bioheat model, *Palestine Journal Of Mathematics*, Vol. 11, pp. 1-11, 2022.

[20] D. Kumar, K. Rai, Three-phase-lag bioheat transfer model and its validation with experimental data, *Mechanics Based Design of Structures and Machines,* Vol. 50, pp. 1-15, 06/19, 2020.
[21] R. Verma, S. Kumar, Computational Study On Skin Tissue Freezing Using Three Phase Lag Bioheat Model, *Journal of Heat Transfer,* Vol. 143, 07/13, 2021.
[22] A. Sur, S. Mondal, M. Kanoria, Influence of moving heat source on skin tissue in the context of two-temperature memory-dependent heat transport law, *Journal of Thermal Stresses,* Vol. 43, 09/30, 2019.
[23] T. Kumari, S. Singh, A numerical study of space-fractional three-phase-lag bioheat transfer model during thermal therapy, *Heat Transfer,* Vol. 51, 08/31, 2021.
[24] S. Singh, P. Saccomandi, R. Melnik, Three-Phase-Lag Bio-Heat Transfer Model of Cardiac Ablation, *Fluids,* Vol. 7, No. 5, pp. 180, 2022.
[25] l. Xiaoya, C. Li, Z. Xue, X. Tian, Investigation of transient thermo-mechanical responses on the triple-layered skin tissue with temperature dependent blood perfusion rate, *International Journal of Thermal Sciences,* Vol. 139C, pp. 339-349, 02/22, 2019.
[26] A. Hobiny, I. Abbas, The Effect of Fractional Derivatives on Thermo-Mechanical Interaction in Biological Tissues during Hyperthermia Treatment Using Eigenvalues Approach, *Fractal and Fractional,* Vol. 7, No. 6, pp. 432, 2023.
[27] M. Sobhy, A. Zenkour, Refined Lord–Shulman Theory for 1D Response of Skin Tissue under Ramp-Type Heat, *Materials,* Vol. 15, pp. 6292, 09/10, 2022.
[28] A. Zenkour, T. Saeed, K. Alnefaie, Refined Green–Lindsay Model for the Response of Skin Tissue under a Ramp-Type Heating, *Mathematics,* Vol. 11, pp. 1437, 03/16, 2023.
[29] l. Xiaoya, L. Pengfei, Q. Qin, X. Tian, The phase change thermoelastic analysis of biological tissue with variable thermal properties during cryosurgery, *Journal of Thermal Stresses,* Vol. 43, pp. 1-19, 05/19, 2020.
[30] R. Tiwari, A. Singhal, R. Kumar, P. Kumar, S. Ghangas, Investigation of memory influences on bio-heat responses of skin tissue due to various thermal conditions, *Theory Biosci,* Vol. 142, No. 3, pp. 275-290, Sep, 2023. eng
[31] Y. Hu, X. Zhang, X.-F. Li, Thermoelastic response of skin using time-fractional dual-phase-lag bioheat heat transfer equation, *Journal of Thermal Stresses,* Vol. 45, pp. 597-615, 06/06, 2022.
[32] Y. Hu, X. Zhang, X.-F. Li, Thermoelastic analysis of biological tissue during hyperthermia treatment for moving laser heating using fractional dual-phase-lag bioheat conduction, *International Journal of Thermal Sciences,* Vol. 182, pp. 107806, 07/21, 2022.
[33] M. Ezzat, Bio-thermo-mechanics behavior in living viscoelastic tissue under the fractional dual-phase-lag theory, *Archive of Applied Mechanics,* Vol. 91, 09/01, 2021.
[34] A. Zenkour, T. Saeed, A. Aati, Refined Dual-Phase-Lag Theory for the 1D Behavior of Skin Tissue under Ramp-Type Heating, *Materials,* Vol. 16, pp. 2421, 03/17, 2023.
[35] Q. Zhang, Y. Sun, J. Yang, Thermoelastic responses of biological tissue under thermal shock based on three phase lag model, *Case Studies in Thermal Engineering,* Vol. 28, pp. 101376, 08/01, 2021.
[36] H. H. Pennes, Analysis of Tissue and Arterial Blood Temperatures in the Resting Human Forearm, *Journal of Applied Physiology,* Vol. 85, No. 1, pp. 5-34, 1998.
[37] D. Y. Tzou, A Unified Field Approach for Heat Conduction From Macro- to Micro-Scales, *Journal of Heat Transfer-transactions of The Asme,* Vol. 117, pp. 8-16, 1995.
[38] D. Y. Tzou, 2014, Macro-to microscale heat transfer: the lagging behavior, John Wiley & Sons,
[39] A. M. Allehaibi, A. M. Zenkour, Magneto-Thermoelastic Response in an Infinite Medium with a Spherical Hole in the Context of High Order Time-Derivatives and Triple-Phase-Lag Model, *Materials,* Vol. 15, No. 18, pp. 6256, 2022.
[40] A. M. Zenkour, On Generalized Three-Phase-Lag Models in Photo-Thermoelasticity, *International Journal of Applied Mechanics,* Vol. 14, No. 02, pp. 2250005, 2022.
[41] A. Zenkour, Thermal diffusion of an unbounded solid with a spherical cavity via refined three-phase-lag Green–Naghdi models, *Indian Journal of Physics,* Vol. 96, 03/19, 2021.
[42] A. Zenkour, Wave propagation of a gravitated piezo-thermoelastic half-space via a refined multi-phase-lags theory, *Mechanics of Advanced Materials and Structures,* Vol. 27, pp. 1-12, 02/18, 2019.
[43] H. M. Youssef, N. A. Alghamdi, Three-dimensional biological tissue under high-order effect of two-temperature thermal lagging to thermal responses due to a laser irradiation, *Vibroengineering Procedia,* Vol. 22, pp. 112-117, 2019.
[44] H. Youssef, R. Salem, The dual-phase-lag bioheat transfer of a skin tissue subjected to thermo-electrical shock, *Journal of Engineering and Thermal Sciences,* Vol. 2, 10/25, 2022.
[45] K.-C. Liu, Y.-N. Wang, Y.-S. Chen, Investigation on the Bio-Heat Transfer with the Dual-Phase-Lag Effect, *International Journal of Thermal Sciences,* Vol. 58, pp. 29–35, 08/01, 2012.

[46] K. Rai, S. Rai, Effect of metabolic heat generation and blood perfusion on the heat transfer in the tissues with a blood vessel, *Heat and mass transfer,* Vol. 35, No. 1, pp. 75-79, 1999.
[47] K.-C. Liu, Nonlinear behavior of thermal lagging in concentric living tissues with Gaussian distribution source, *International Journal of Heat and Mass Transfer - INT J HEAT MASS TRANSFER,* Vol. 54, pp. 2829-2836, 06/01, 2011.
[48] D. Y. Tzou, Experimental support for the lagging behavior in heat propagation, *Journal of Thermophysics and Heat Transfer,* Vol. 9, No. 4, pp. 686-693, 1995.
[49] H. Askarizadeh, H. Ahmadikia, Analytical study on the transient heating of a two-dimensional skin tissue using parabolic and hyperbolic bioheat transfer equations, *Applied Mathematical Modelling,* Vol. 39, No. 13, pp. 3704-3720, 2015/07/01/, 2015.
[50] P. Hooshmand, A. Moradi, B. Khezry, Bioheat transfer analysis of biological tissues induced by laser irradiation, *International Journal of Thermal Sciences,* Vol. 90, pp. 214-223, 2015/04/01/, 2015.
[51] A. McBride, S. Bargmann, D. Pond, G. Limbert, Thermoelastic modelling of the skin at finite deformations, *J Therm Biol,* Vol. 62, No. Pt B, pp. 201-209, Dec, 2016. eng